Supporting Online Materials

Electron Microscopy Observation of TiO_2 Nanocrystal Evolution in High-Temperature Atomic Layer Deposition

Jian Shi,[1,†] Zhaodong Li,[1] Alexander Kvit,[1,2] Sergiy Krylyuk,[3] Albert V. Davydov,[3] Xudong Wang[1,*]

1. Department of Materials Science and Engineering, University of Wisconsin-Madison

2. Materials Science Center, University of Wisconsin-Madison

3. National Institute of Standards and Technology

† Current address: School of Engineering and Applied Sciences, Harvard University

* Email: xudong@engr.wisc.edu

S1: Experimental Details of Materials Growth

(1) Setup and Conditions of Atomic Layer Deposition (ALD)

TiO_2 thin films and nanorods (NRs) were grown in a home-made ALD facility. Separated exposures of gaseous $TiCl_4$ and H_2O vapors were controlled by solenoid valves and adjusted by fine tuning the precursor tank temperature. In details, substrates [Si nanowires (NWs) or ZnO NWs] were placed at the center of the ALD chamber (stainless steel tube with a diameter of 2 inch) and 10 cm downstream away from the precursor injection nozzle. During the growth, a constant flow of 40 sccm N_2 was applied into the chamber as the carrier gas, which provided a background pressure of 2.7 Torr. The chamber temperature was maintained at 300 ℃ or 600 ℃. In a typical TiO_2 NRs (at 600 ℃) process, $TiCl_4$ and H_2O vapor precursors were pulsed into the chamber for 1 s each and separated by purging N_2 for 60 s. Thus, one growth cycle includes 1 s of H_2O pulsing + 60 s of N_2 purging + 1 s of $TiCl_4$ pulsing + 60 s of N_2 purging. For TiO_2 polycrystalline thin film (at 300 ℃) growth, the $TiCl_4$ and H_2O precursor pulses were both 0.5 s and separated by 60 s N_2 purging. After growth, the chamber cooled down to room temperature naturally under N_2 flow. To prepare the different stages of nanostructure/film, growth was interrupted at the ALD growth cycles of 2, 5, 10, 20, 25, 35, 50, 75, 100, 200, 300 and 400. Figure S1 presents the low-magnification scanning transmission electron microscopy (STEM) images of TiO_2 morphologies on Si nanowires (NWs) grown in different ALD cycles at 600 ^oC. All nanostructures observed and compared were prepared under the same ALD growth conditions.

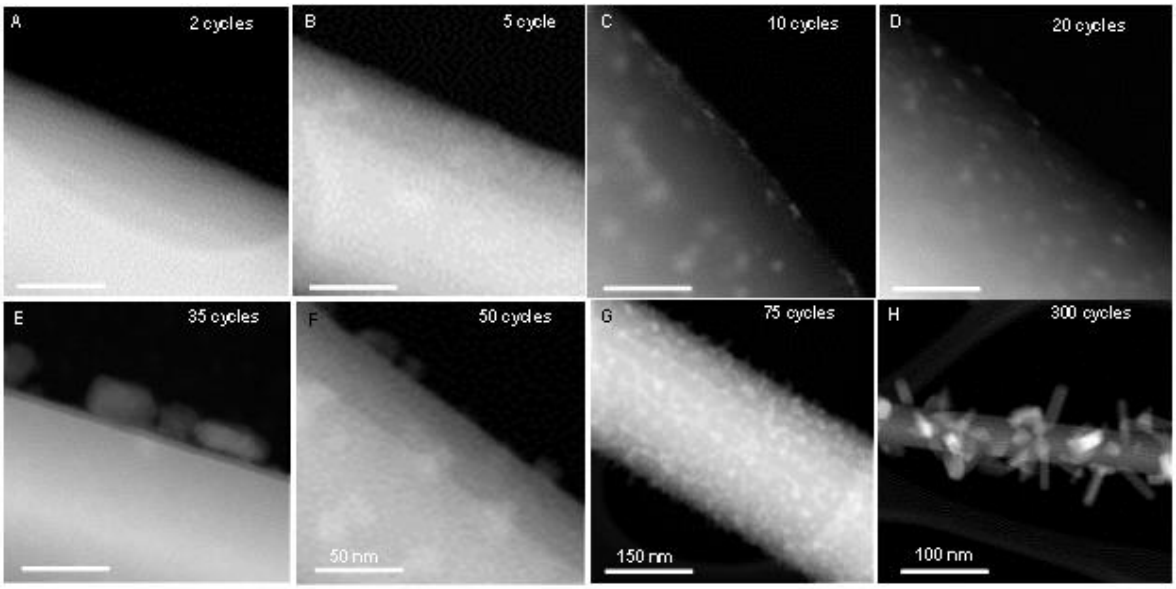

Fig. S1. Low magnification of STEM images at different ALD stages (scale bars are 20 nm unless otherwise noted).

(2) Growth of ZnO NWs by Chemical Vapor Deposition (CVD)

A horizontal tube furnace system was used to perform the vapor deposition of ZnO NW. A small quartz tube 25 cm in length and 1.6 cm in inner diameter was used to support the precursor and substrate and increase the vapor concentration. In a typical process, ZnO powder (0.3 g) and graphite powder (0.3 g) were mixed and ground together and placed in a quartz boat positioned 5 cm from one end in the quartz tube. A 500-nm-thick GaN epilayer covered sapphire substrate was used for ZnO nanostructure deposition. The substrates were 8 cm away from the source boat. This small quartz tube was then placed into a large alumina tube in the tube furnace with the source boat aligned at the center of the tube furnace and the substrates located on the downstream side of the carrier gas. The carrier gas used throughout the experiments was 1% oxygen balanced by high purity argon. First, the furnace was quickly increased to 925 ℃ at a ramp rate of 50 ℃/min. When the temperature reached 400 ℃, the carrier gas was introduced into the deposition system with a flow rate of 50 sccm and the system pressure was brought to 20 Torr. Then the furnace temperature was held at 925 ℃ for 30 min for ZnO NW deposition. At this temperature, according to the temperature profile of this furnace, the local substrate temperature was 900 ℃. Finally, the furnace was turned off and the system was allowed to cool down naturally without changing the system pressure and carrier gas flow.

(3) Growth of Si NW by CVD

Gold-catalyzed Si NWs were grown in a home-built hot-wall CVD system at 900 ℃ and 80 kPa (600 Torr) reactor pressure using 30 sccm (standard cm^3/min) of silicon tetrachloride and 200 sccm of hydrogen diluted with nitrogen to a total flow rate of 1000 sccm. $SiCl_4$ vapor was delivered by nitrogen carrier gas through a bubbler with liquid $SiCl_4$ held at 15 ℃ and 104 kPa (780 Torr). Au nanoparticles (100 nm in diameter) dispersed on poly-L-lysine-functionalized Si(111) substrate were utilized to facilitate the vapor-liquid-solid (VLS) growth mechanism of the NWs.

(4) Characterization

All HR-HAADF-STEM, TEM, HRTEM images, and EELS characterization were conducted in a C_s-corrected FEI Titan microscope operated at 200 kV. HAADF STEM images were collected with a 24.5 mrad probe semiangle, and 24.5 pA probe current. *in-situ* TEM heating holder from Hummingbird was used to dynamically observe the crystal structural evolution of TiO_2 NRs heated to be 600 ℃.

S2: Crystal Structure of Small Crystallites

One distinguishable feature of HRTEM (high resolution transmission electron microscopy) image from HR-STEM (high resolution scanning transmission electron microscopy) is that it provides phase contrast to differentiate the amorphous phase from crystalline region. As a supplemental instrumentation, we apply HRTEM to confirm the crystal structure of small crystallites grown at 35 cycles of 600 ℃ ALD. HRTEM image (Fig. S2) indicates that there is always a thin layer of amorphous TiO_2 wrapping the crystallites, which is often a few angstroms thick. Each polycrystalline assemblage is composed of a few individual small crystallites.

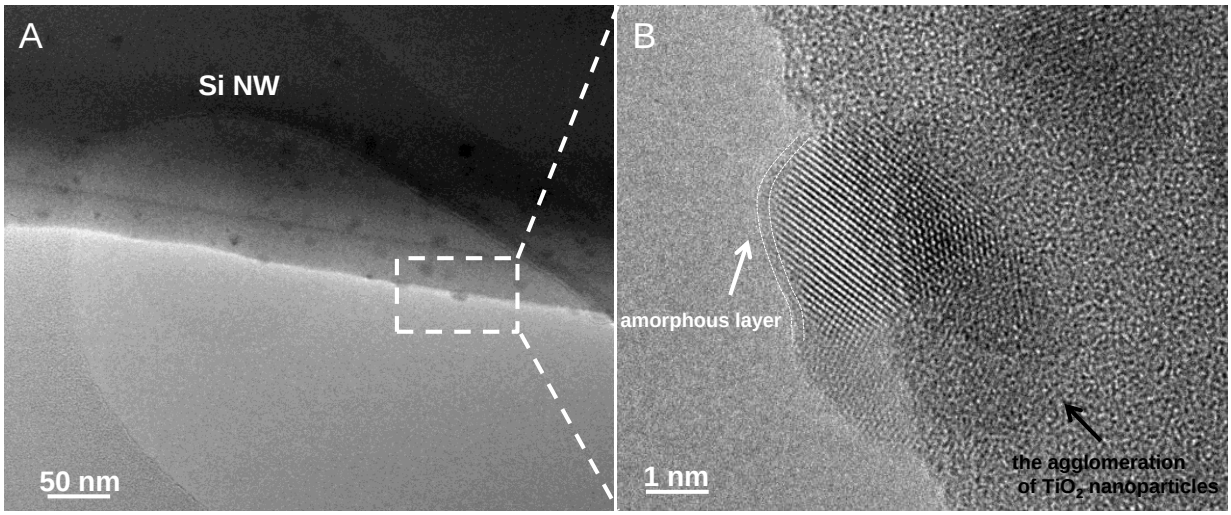

Figure S2. TEM images of 35 cycles ALD growth at 600 ℃. (A) Size distribution of 35 cycles ALD growth results on Si NWs. **(B)** An amorphous sub-nanometer-thick TiO_2 layer covering the surface of the crystallites assemblage.

S3: Conformal NRs Growth by 600 ^{o}C ALD

CVD Si NWs arrays were used as growth substrates to investigate the conformity and size distribution of 600 ℃ ALD TiO_2 NRs. Length of these Si NWs is usually above 10 μm and their diameters range from a few tens of nanometers to several hundred nanometers. In a very typical growth recipe of 1 s of H_2O pulsing + 60 s of N_2 purging + 1 s of $TiCl_4$ pulsing + 60 s of N_2 purging, conformal NRs coating was achieved across the whole Si NW axial direction. Figure S3 shows that the density and size of TiO_2 NRs acquired from the base region of Si NWs is more or less similar to the top rim of NWs, demonstrating a powerful technique/growth mode for hierarchical NW-NR structure fabrication.

The merit of this NR growth approach is the ability to deposit high density NR arrays inside highly confined submicrometer spaces. In our previous work, we demonstrated the deposition of TiO2 NRs around dense Si NWs forest, as shown in Fig. S4 (obtained from our previous publication *Nano Letters, 11, 3413-3419, 2011*). This structure offers tremendous surface area per unit substrate area as well as excellent charge transport property. Therefore, they are a very promising 3D nanostructure for developing high-performance photovoltaic and photoelectrochemical electrodes.

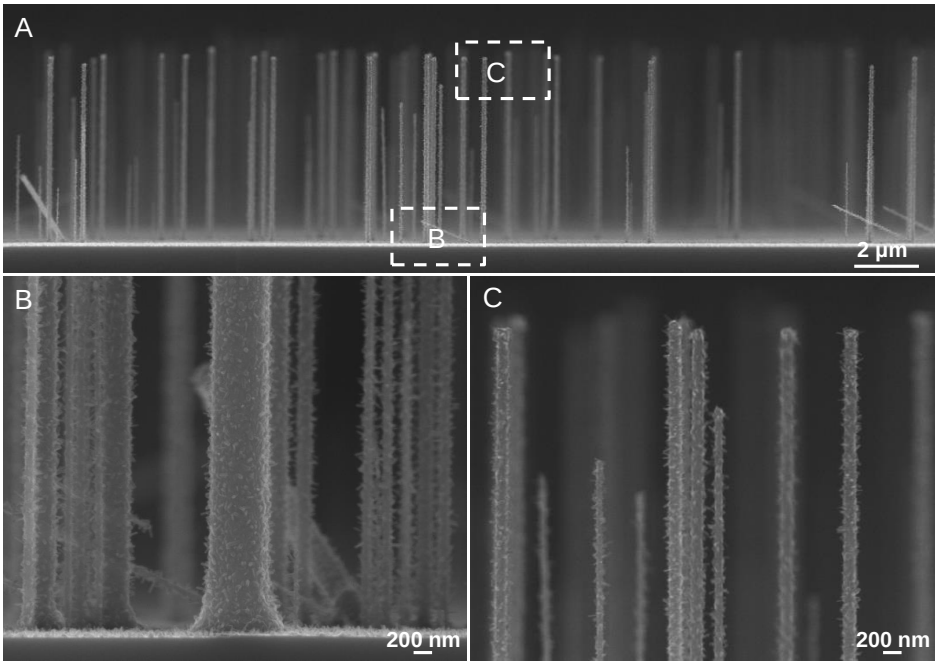

Figure S3. SEM images of 400 cycles ALD growth of TiO_2 NRs on single crystalline Si NWs arrays. (A) Low magnification SEM image of Si NWs arrays. Growth of TiO_2 NRs on the base **(B)** and tip rim **(C)** of Si NWs.

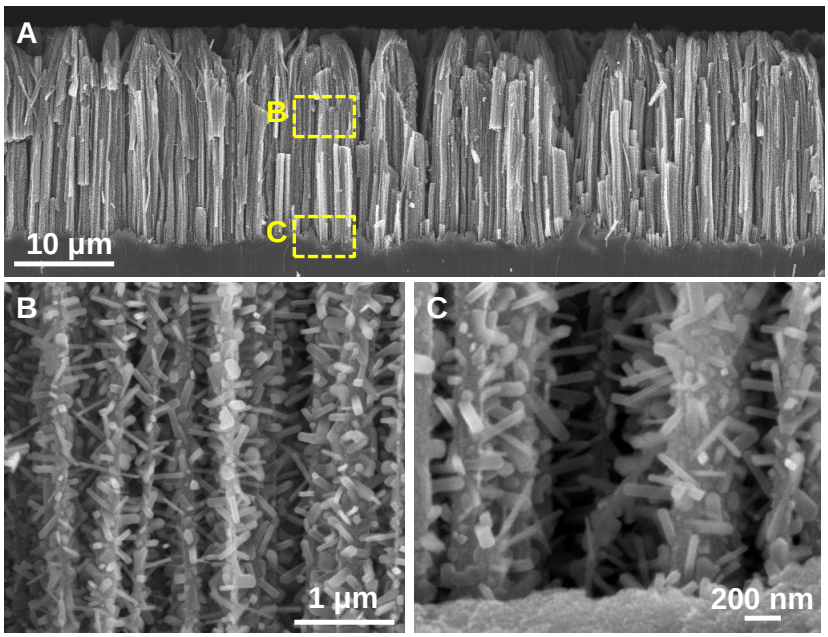

Figure S4. SEM images of TiO_2 NRs grown inside high-density Si NW forest. (**A)** Cross-section of vertical Si NW arrays covered with TiO_2 NRs. The Si NWs are ~25 μm long and the top ~5 μm region was bundled together. **(B, C)** The middle and bottom portions of Si NWs showing dense and uniform coverage of TiO2 NRs along the entire NW length. (from reference *Nano Letters, 11, 3413-3419, 2011*).

S4: Phase Transformation and Self-organization of Crystallites

In order to further confirm the amorphous phase of the small particles we observed on the surface of Si NWs by HR-STEM, HRTEM was utilized for phase identification. As shown in Fig. S5A, these small (~ 1nm in width) amorphous particles have a relatively sparse distribution on the Si NW surfaces. Because HRTEM is not Z-contrast-based, often only half of these amorphous particles' body would show up from the Si NW. Their amorphous structure can be clearly evidenced from the HR image (Fig. S5B). As the growth proceeds to 25 cycles, individual crystalline TiO_2 particle is identified as shown in Fig. S5C, which is believed to be transformed from the amorphous particles formed in the earlier stages. An amorphous layer can also be spotted on the surface of the single crystalline particles. At 25 cycles, polycrystalline assemblage is also observed, which consists of a few small particles aligning along the same orientation (Fig. S5D), suggesting the occurrence of self-organization of TiO_2 crystallites by following oriented attachment growth mechanism.

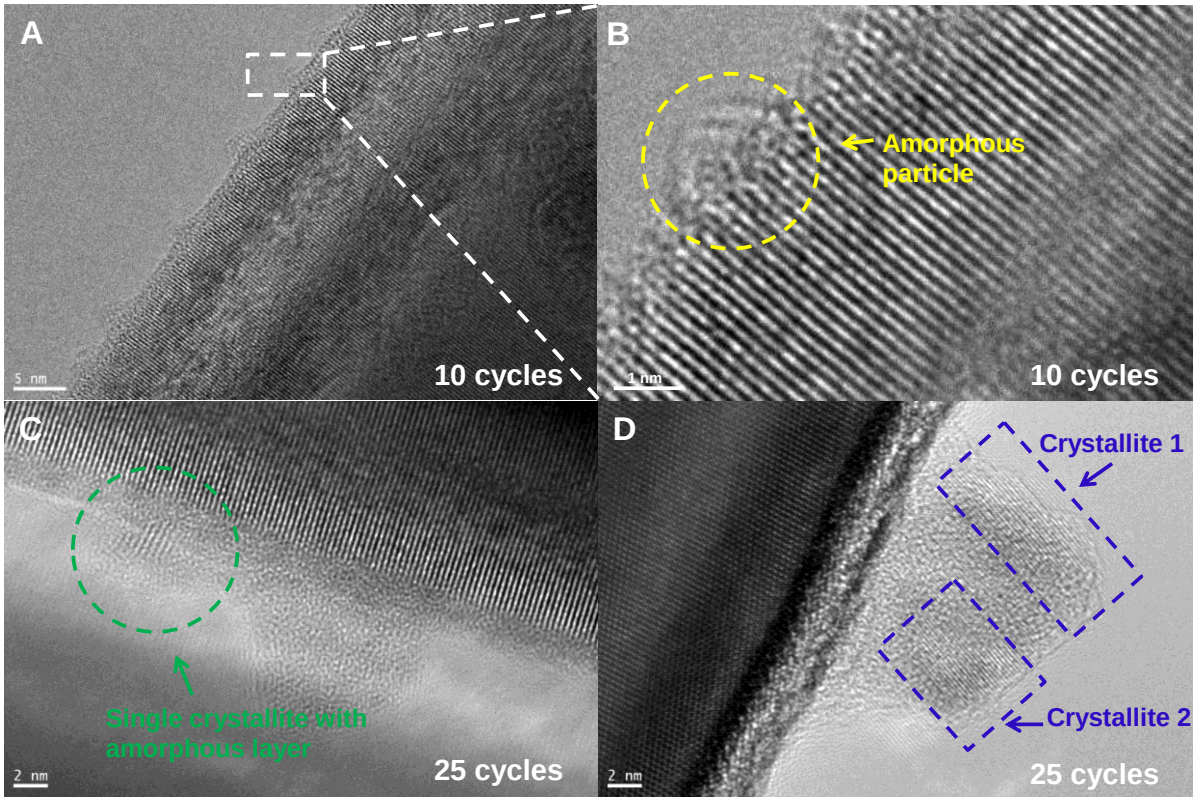

Figure S5. Phase transformation and self-organization of crystallites. (A, B) High resolution TEM images of amorphous TiO_2 nanoparticles growing on single crystalline Si NWs after 10 cycles ALD growth at 600 ℃. **(C)** Presence of TiO_2 crystallites coated by a thin layer of amorphous film after 25 cycles growth of ALD at 600 ℃. **(D)** Self-organization of small crystallites along certain crystallographic orientation suggesting the concurrence of oriented attachment growth mechanism.

S5: Supportive Evidence of Vapor Phase Oriented Attachment

To further evidence the evolution of TiO_2 NRs embryos follows the vapor phase oriented attachment mode, we attempt to simulate this process in TEM chamber and simultaneously monitor the morphology development (Fig. S6). We firstly grew a 25 cycles of ALD amorphous TiO_2 layer at 120 ℃ with extend water pulse (2 s) on silicon nitride membrane TEM grid, then immediately loaded the sample inside TEM chamber for electron beam radiation. Right after 1 minute TEM beam radiation, several small TiO_2 crystallites formed a chain by aligning them along one certain orientation. This chain became larger when the radiation time reached 2 minutes and finally a NR embryo started to present after 5 minutes. This observation is supportive evidence to the vapor-phase oriented attachment growth mechanism.

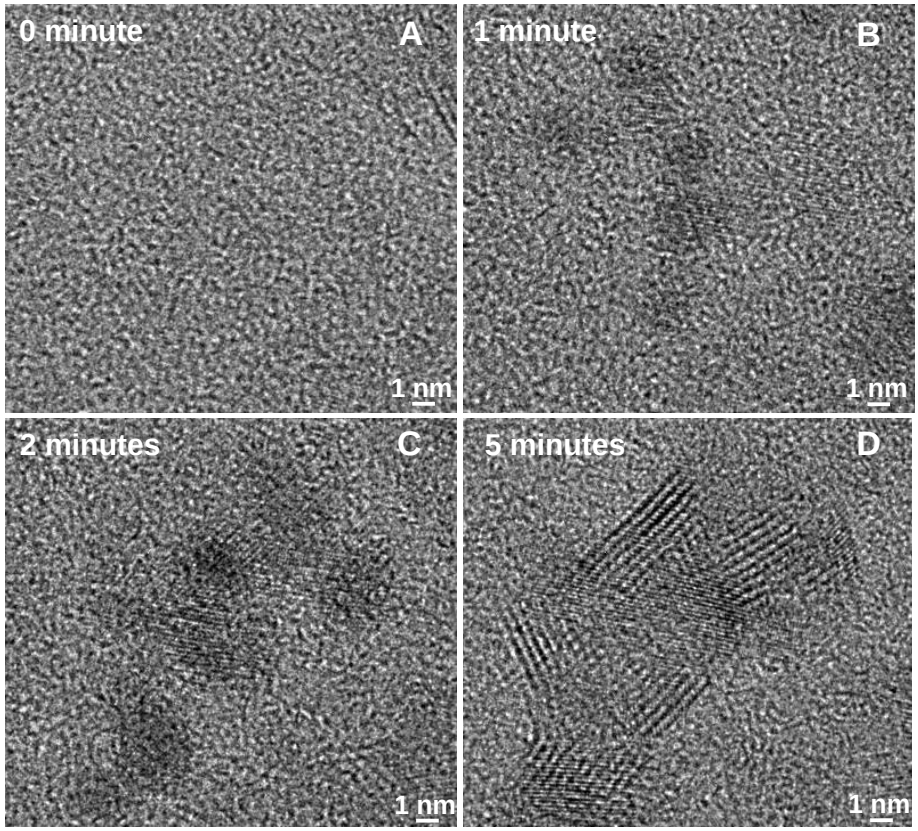

Figure S6. Oriented attachment growth mechanism simulated by TiO_2 nanoparticles grown on silicon nitride membrane TEM grid. (A) As-coated amorphous TiO_2 film on SiN membrane prior to electron beam illumination. **(B)** Formation of a nanochain by self-organization of small TiO_2 crystallites along one crystallographic orientation after 1 minute electron beam radiation. **(C)** Propagation of the nanochain formed at stage (B) by attaching more small crystallites after 2 minutes electron beam radiation. **(D)** The continuous expanding and elongation of the nanochain by more oriented attachment growth after 5 minutes illumination. The superlattice formed in (D) is believed to be consequence of the imperfect crystallite alignment/organization.

S6: The Emergence of Rutile Structure

According to Ostwald-Lussac Law, eventually we should expect the presence of rutile structure after a very long growth period. To search for such evidence, we have prepared the ALD TiO_2 structures grown at 660 cycles, 900 cycles and 1200 cycles at 600 ℃. X-ray diffraction (XRD) was conducted to reveal the phase evolution from anatase to ultimate rutile structure. It was found that at 660 cycles, the TiO_2 is still pure anatase (Fig. S7). When the growth proceeds to 900 cycles, the rutile phase starts to appear though still as the minority. As growth goes to 1200

cycles, the relative ratio of rutile to anatase increases illustrated by the intensities of their corresponding XRD peaks. Such finding fits in the derivation from Ostwald-Lussac Law.

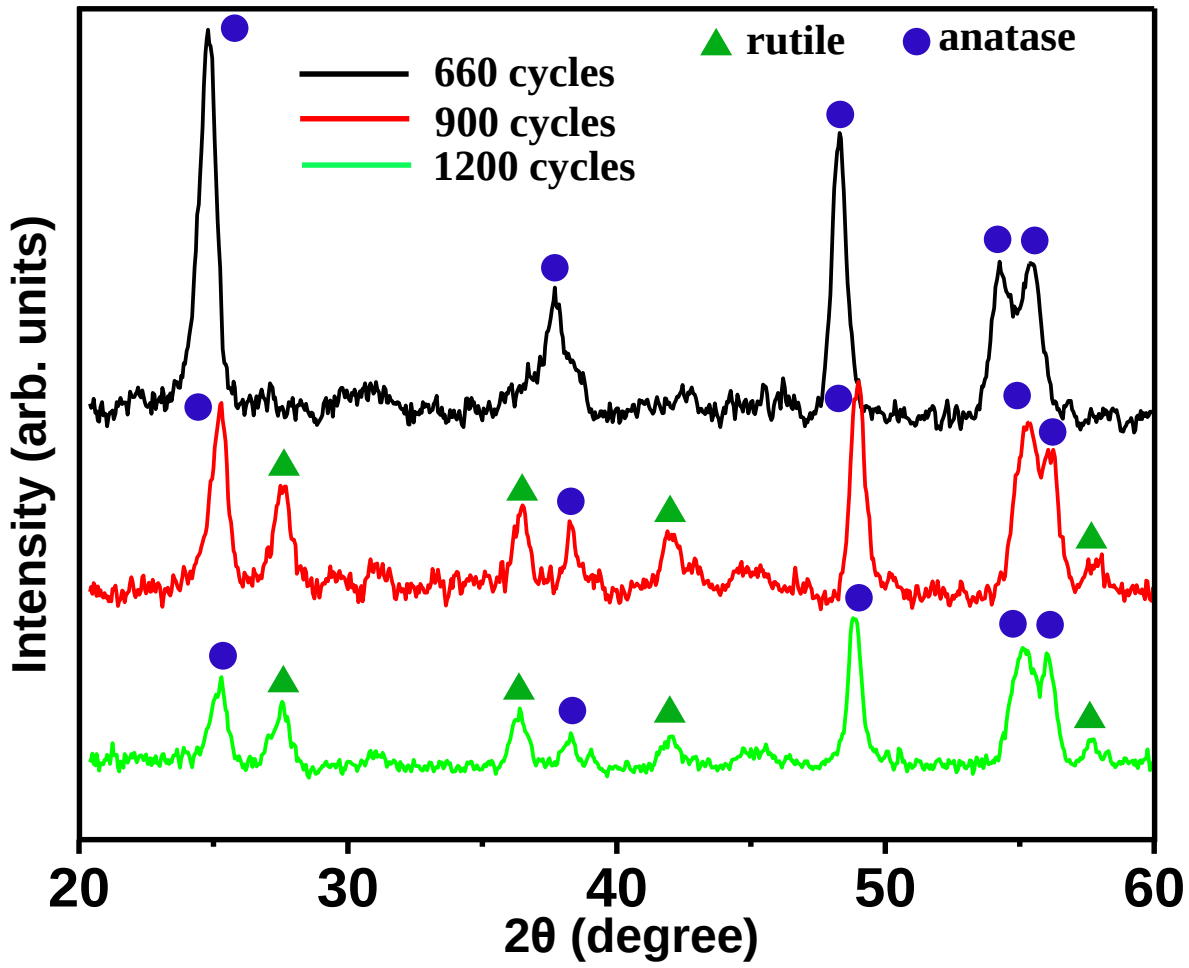

Figure S7. X-ray diffraction spectra of TiO_2 NRs grown at 660, 900 and 1200 cycles. At 660 cycles, the NRs were still pure anatase phase while at 990 cycles, the rutile phase started to appear and its relative amount to the anatase phase further increased at 1200 cycles.

S7: Derivation of Nucleation Rates

The general nucleation rate is given by,

$$J_n = Aexp(-\frac{\Delta g_n}{k_B T}) ,$$

where k_B is Boltzmann constant, T is the nucleation temperature, A is a constant and Δg_n is the nucleation barrier.

For a heterogeneous nucleation, nucleation barrier is,

$$\Delta g_n = \frac{(16/3)\pi\gamma^3 v^2}{(k_B T ln S)^2},$$

where v is the molecular volume, ln$S$ is the supersaturation, and γ is the surface free energy of nucleus, which is given by,

$$\gamma = \gamma_{gc}\{1 - (\gamma_{gs} - \gamma_{sc})/2\gamma_{gc}\},$$

According to the 10- and 20-cycle growth results, most amorphous nanoparticles exhibit very large contact angle on the NW surface. Thus to first order approximation, γ is simplified to be γ_{gc} in our subsequent calculations. The nucleation rate therefore is obtained as,

$$J_n = Aexp(-B\frac{\gamma^3}{(lnS)^2}),$$

where B is a constant.

S8: Secondary Nucleation on Single Crystalline TiO_2 Surface

The emergence of single crystalline TiO_2 NRs inevitably provides a new growth surface for ALD TiO_2 film/crystal nucleation. The TiO_2 amorphous-crystalline percolated shell on the TiO_2 NR body is therefore believed to be the result of the expected secondary nucleation deposition, which also follows the Ostwald-Lussac Law. High resolution electron energy loss spectroscopy (EELS) map and line scan revealed that such percolated shell was much less compact than the NR body (Fig. S8).

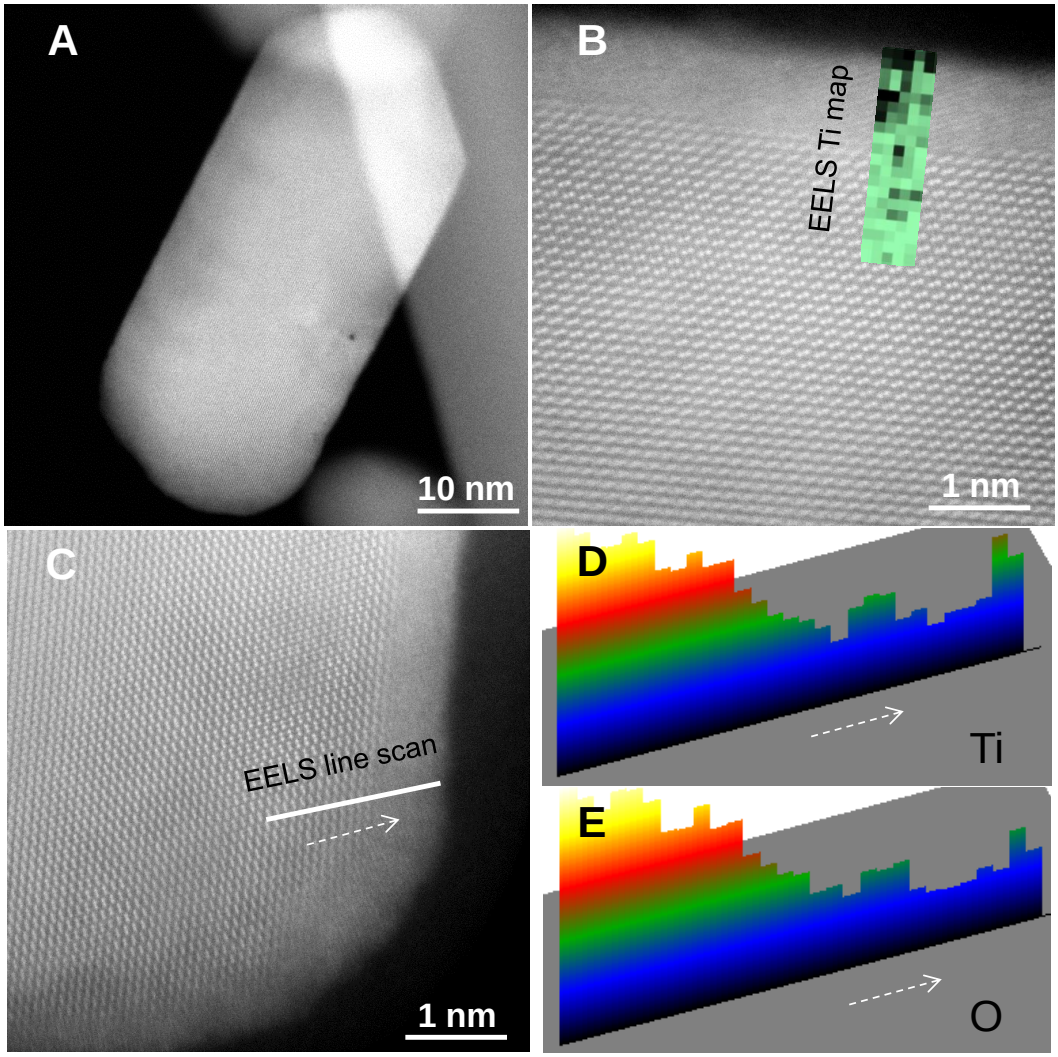

Figure S8. EELS characterization of 100 cycles TiO_2 NRs grown at 600 ℃ ALD. (A) Low magnification STEM image showing the overall morphology of the NR anchoring on the Si NW. **(B)** Atomistic EELS Ti map across the percolated film-single crystalline region of NR with brighter color illustrating more Ti and darker color for less Ti. **(C)** HR STEM image of the TiO2 NR covered with an amorphous layer, where EELS line scan is indicated. **(D, E)** are the Ti and O EELS signal profiles, respectively, along the NR edge. They demonstrate that the percolated surface film is much less compacted than the NR body.

S9: TEM Beam Illumination-Induced NR Growth

To investigate the NR growth mode during intermediate ALD cycles (75 cycles) and explore the evolution of the percolated TiO_2 shells formed in the secondary nucleation process, we grew a TiO_2 NR embryo at 75 cycles *via* 600 ℃ ALD and then immediately loaded it into TEM chamber for characterization. Here, TEM electron beam was used as to radiate the TiO_2 crystal

and activate the recrystallization. Meanwhile, HRTEM images were captured every 1 minute after beam radiation. The electron beam may induce local heating due to the poor thermal conductivity of the sample, or knock-out damage that largely increases the mobility of individual atoms. Either effect would facilitate the recrystallization of TiO2 and may recover the NR evolution process. EELS maps (not shown here) demonstrate that the NR investigated usually consist of two major regions: thick and thin (Fig. S9A). Along with the time of beam radiation, the thick region propagates while the thin part shrinks (Fig. S9B and C). The width of NR is found to be narrowed down after 2 minutes beam heating suggesting the sacrificing of percolated TiO_2 shells for NR growth.

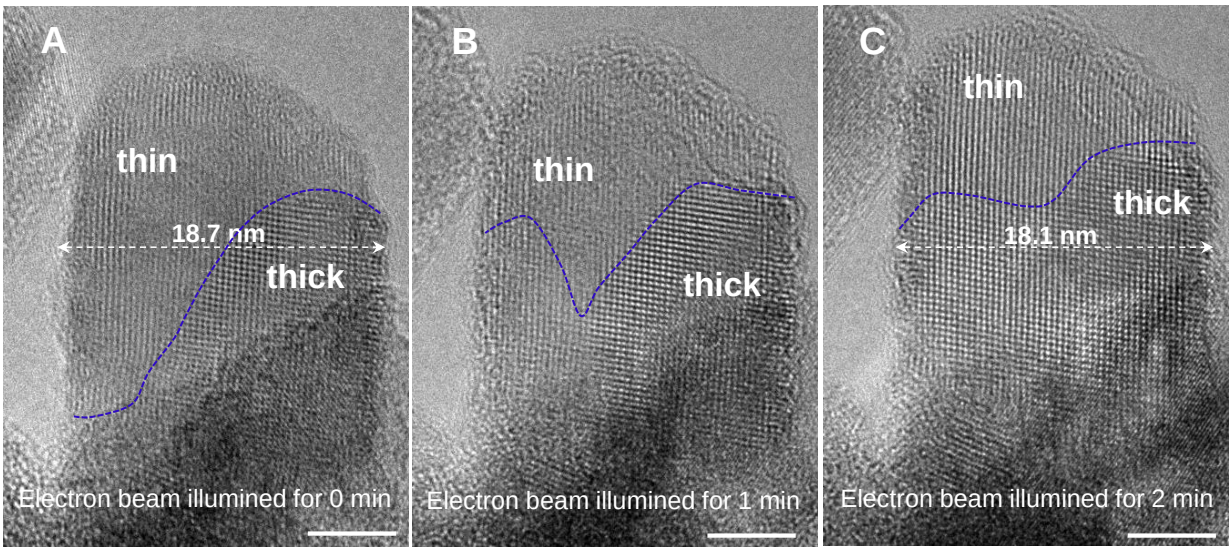

Figure S9. Electron beam-induced 75 cycles NR growth during TEM chamber. (A) A HRTEM image of TiO_2 NR prior to electron beam illumination. The NR consists of three distinct regions: thick region, thin region and percolated film sidewalls. The thickness of the NR at the indexed location at this stage is 18.7 nm. Blue dash line is used to outline the boundary between the thick and thin regions. **(B)** With 1 minute TEM beam illumination, the thick region advances while the thin region shrinks. **(C)** After 2 minutes beam illumination, the thick region keeps propagating and thin region becomes less. The diameter of the NR at the specific location at this stage is found to be smaller (18.1 nm) indicating the consumption of percolated regions. All scar bars are 5 nm.

S10: *In-situ* Thermal Heating-Induced Crystal Growth

As discussed in the main text and previous reference (*Nano Letters, 11, 3413-3419, 2011*), the TiO_2 NR (002) facet is the active growth front. By *in situ* heating of a TiO_2 NR with its (002) facet coated by the percolated TiO_2 shell, we attempted to directly observe the growth process on the active facet (Fig. S10). To enable such experiment, we firstly grew TiO_2 NRs via 400 cycles

ALD then coated the NRs with a 5-cycle ALD TiO_2 film at 300 ℃. Afterwards, we loaded the sample into TEM chamber anchored on a TEM heating holder. The temperature of the NR was ramped to 600 ℃ in 1 minute and kept for 5 minutes. Right before and after annealing, HRTEM images were captured. It shows that small crystallites on the (002) surface prior to annealing realigned themselves to incorporate on the NR (002) facet after annealing while other facets of NR did not exhibit sensible change. Such observation confirms that (002) is the active growth plane, which is a consequence of its high surface free energy and consistent with the oriented attachment growth mechanism.

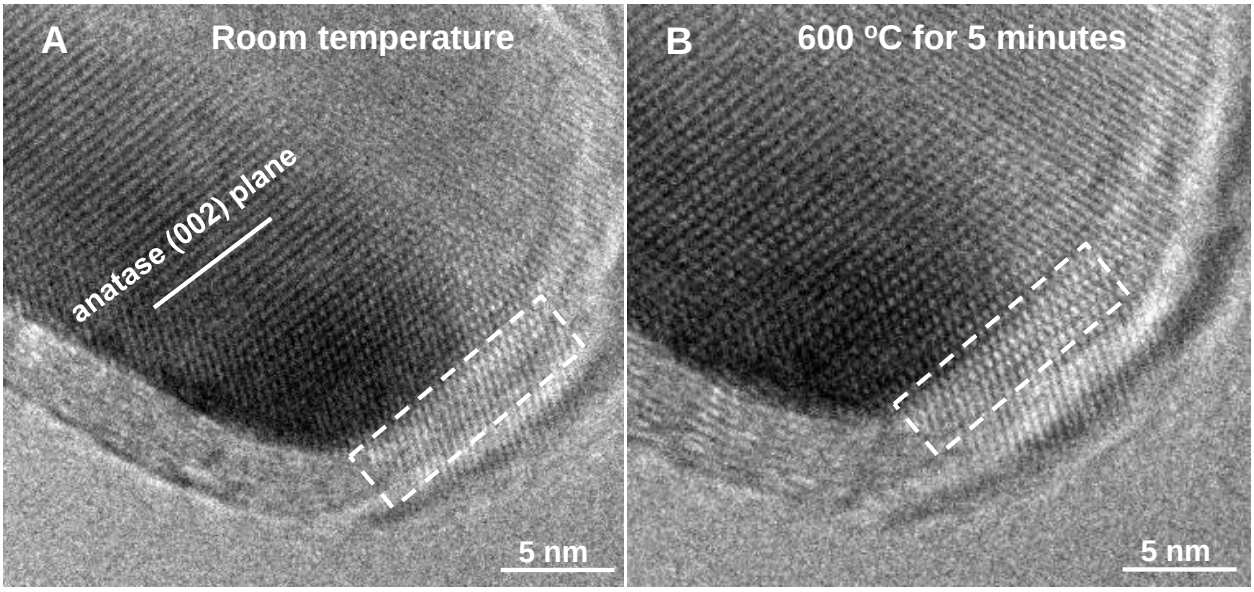

Figure S10. *in situ* heating of 400 cycles TiO_2 NR in a TEM heating holder. (A) HRTEM image of NR tip at room temperature prior to thermal heating. Dash rectangle indicates the existence of a percolated layer on the NR tip. **(B)** After ramping the temperature to 600 ℃ in 1 minute and then holding at 600 ℃ for 5 minutes, the percolated film transformed to a part of single crystalline anatase phase, suggesting the self-organization of small crystallites onto NR body for oriented attachment growth during thermal heating. The thick amorphous layer is due to the carbon deposition during TEM imaging and thermal heating.